

Closure of the sea surface height budget with a Stokes offset

Jörn Callies^a, Charly de Marez^{a,b}, Jinbo Wang^c, and Bruce Haines^d

^aCalifornia Institute of Technology

^bUniversity of Iceland

^cTexas A&M University

^dJet Propulsion Laboratory, California Institute of Technology

Abstract

The sea surface height budget, obtained by integrating hydrostatic balance over the water column, relates sea surface height variations to variations of the seafloor pressure, density in the water column, and atmospheric surface pressure. This budget is crucial for calibrating and interpreting satellite altimetry measurements. It only holds once non-hydrostatic surface gravity waves are averaged out, however, which complicates an observational closure of the budget. Using data from the California Current System, this study demonstrates that the budget closes to within understood uncertainties if GPS buoy measurements of surface height are interpreted as Lagrangian measurements. The buoy largely follows wave motion and spends slightly more time near wave crests than troughs. The associated Stokes offset, which reaches a maximum of 15 cm in these observations, must be accounted for in the Eulerian sea surface height budget.

1 Introduction

Precise measurements of the sea surface height from space have drastically advanced global oceanography. Satellite altimetry captures the geostrophic circulation, which consists of gyres, boundary currents, jets, and ubiquitous mesoscale eddies (Wunsch and Stammer, 1998; Chelton et al., 2011). Altimetry data are the basis of accurate maps of

the external tides (Le Provost et al., 1995); they have revealed the long-range propagation of internal tides (Ray and Mitchum, 1996); and they can be used to infer where the external tides lose energy to internal tides and dissipation (Egbert and Ray, 2000), with important implications for the circulation and stratification of the deep ocean (Munk and Wunsch, 1998). Furthermore, altimetry data constitute the backbone of estimates of global sea level rise (Cazenave and Llovel, 2010).

The Surface Water and Ocean Topography (SWOT) mission, launched in December 2022, measures the sea surface height with unprecedented precision (Fu et al., 2024). To evaluate these new measurements, a set of moorings was deployed in the California Current System. These moorings measure density fluctuations in the water column, the vertical integral of which dominates the non-tidal sea surface signal (Wang et al., 2022). Some of these moorings also carry GPS buoys that directly measure the sea surface height using recently developed technology (Haines et al., 2017; Desai et al., 2018; Haines et al., 2019), adding redundancy to the evaluation of SWOT data. A comparison between these GPS buoy data and altimetric measurements should be made with caution, however, because the buoy measurements are subject to a Stokes offset due to surface gravity waves (Longuet-Higgins, 1986). The buoys move mainly with the gravity wave orbit, spending slightly more time near the wave crest than near the wave trough, shifting the Lagrangian mean position upward relative to the Eulerian mean sea surface height. Using data from a pre-launch deployment, we demonstrate the importance of this offset by closing the sea surface height budget, which is obtained by integrating the hydrostatic balance over the water column (Gill and Niiler, 1973).

2 The sea surface height budget

At sufficiently large horizontal scales, ocean flows have a small aspect ratio and nearly satisfy hydrostatic balance,

$$\frac{\partial p}{\partial z} = -\rho g, \quad (1)$$

where p is pressure, ρ is density, g is the gravitational acceleration, and z is the vertical coordinate. Integrating this balance from the seafloor at $z = -H$ to the surface at $z = h$ and denoting the bottom and surface pressures as p_b and p_a , respectively, we obtain

$$p_b - p_a = g \int_{-H}^h \rho \, dz \simeq \rho_0 g h + g \int_{-H}^0 \rho \, dz. \quad (2)$$

In the approximation, we use the fact that surface density variations away from the reference $\rho_0 = 1024 \text{ kg m}^{-3}$ are small compared to the reference value and that the sea surface height variations h are small compared to the reference water depth H . This integrated hydrostatic balance can be written as the sea surface height budget

$$h - h_a - h_b = h_s - H, \quad (3)$$

where

$$h_a = -\frac{p_a}{\rho_0 g}, \quad h_b = \frac{p_b}{\rho_0 g}, \quad h_s = -\int_{-H}^0 \frac{\rho - \rho_0}{\rho_0} dz. \quad (4)$$

The terms in the sea surface height budget are the surface height h itself, the barometric correction h_a (also known as the “inverted barometer” effect; Wunsch and Stammer, 1997), the height equivalent to the bottom pressure h_b , the steric height h_s , and the mean water depth H . If we remove the time mean of all quantities, we obtain

$$h' - h'_a - h'_b = h'_s. \quad (5)$$

Closure of this budget to within understood uncertainties would increase our confidence in the measurements used to estimate each term. It would also increase our confidence in estimates of any one term as a residual of this budget, for example, estimates of the sea surface height from a combination of measurements of bottom pressure and steric height, supplemented with an estimate of atmospheric pressure from a surface measurement or reanalysis product.

We demonstrate here that this budget can be closed using measurements from a field experiment in the California Current System that was conducted from September 2019 to January 2020 in anticipation of the SWOT launch (cf., Wang et al., 2022). We use measurements of the sea surface height from a GPS buoy, estimate the barometric correction using atmospheric reanalysis (ERA5), use a bottom pressure recorder, and estimate steric height from a set of 17 CTDs along the mooring line (Fig. 1). We remove the first two weeks of the bottom pressure data because of instrument drift during that period. The mooring was designed as a slack mooring, with the mooring line much longer than the water depth, which minimizes the line tension and allows the surface buoy to follow the surface height. A detailed description of the mooring design and the instrumentation, including a discussion of error sources, is provided by Wang et al. (2022); the mooring used here is the “northern mooring” described there. The only difference in the processing of the GPS data is that we do not apply the empirical correction for an apparent sea

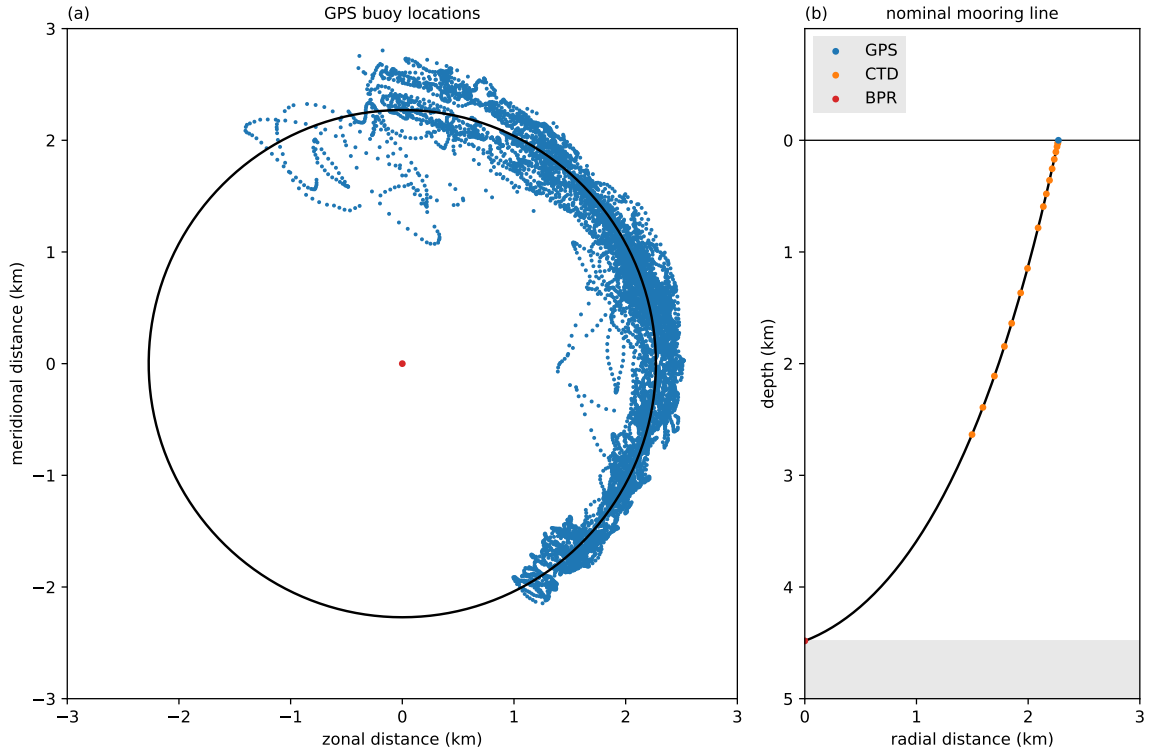


Figure 1: Configuration and position of the mooring in the California Current System. (a) Location of the GPS buoy over the course of the deployment (blue dots), relative to the mooring anchor (red dot, $36^{\circ}07' \text{ N}$, $125^{\circ}08' \text{ E}$), inferred by fitting a circle to the measured GPS surface positions (black circle). (b) Nominal mooring line and sensor positions when the surface buoy is at its mean displacement (black circle).

state bias, which was estimated as 0.018η in Wang et al. (2022), where η is the significant wave height. We argue below that this apparent bias is due principally to the Stokes offset. For all time series, we remove a linear fit over the period during which all observations are available (2019-09-19, 15:00 UTC to 2020-01-19, 15:00 UTC).

The dominant signal on the GPS buoy is that of wind waves and swell (Fig. 2). These are surface gravity waves in the deep-water limit and do not satisfy (1). We must average over them to close the sea surface height budget for the signals produced by larger-scale hydrostatic flows. We average here over 20-minute bins. Because the buoy largely moves with the surface waves in the both the vertical and horizontal directions, a time average over the buoy measurements is closer to a Lagrangian than an Eulerian mean of the sea surface height. For a plane wave and to second order in the wave amplitude a , this

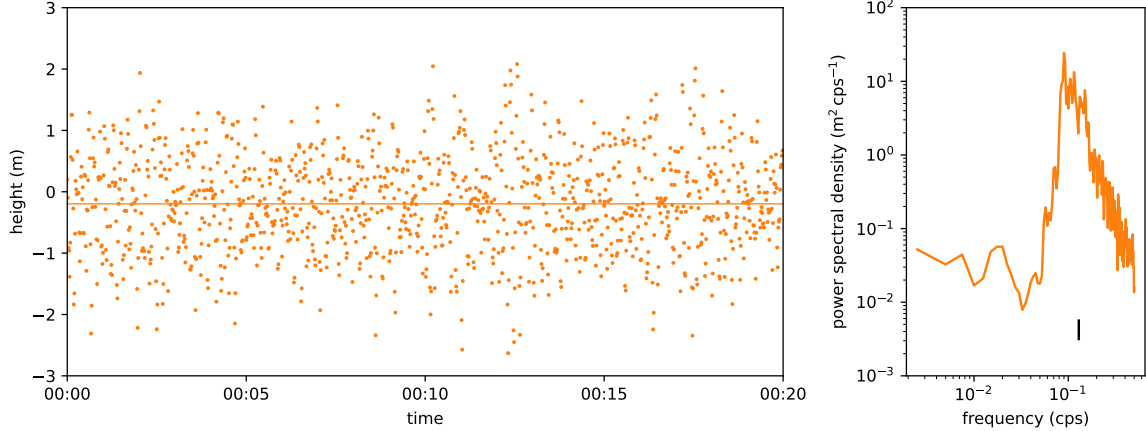


Figure 2: Example surface height signal from the GPS buoy dominated by surface gravity waves. (a) Time series of the barometrically corrected 1 Hz GPS buoy data for the first 20 minutes of 2019-10-11 (UTC), with the mean over this time period $h'_g - h'_a = -19$ cm indicated by the horizontal line. (b) Power spectrum estimated from this time series showing a peak corresponding to the dominant surface gravity waves. The wave period $2\pi/\omega = 7.7$ s estimated from this spectrum is indicated by the black vertical line.

Lagrangian mean differs from the Eulerian mean surface height by the Stokes offset $\frac{1}{2}a^2k$, where k is the wavenumber (e.g., Longuet-Higgins, 1986; Bühler, 2014; Salmon, 2020). The Eulerian mean surface height h and the Lagrangian mean h_g measured by the GPS buoy are therefore related by $h = h_g - \frac{1}{2}a^2k$. For a typical significant wave height of $\eta = 3$ m and a typical wavelength of $2\pi/k = 100$ m, the Stokes offset is $\frac{1}{16}\eta^2k = 3.5$ cm, where we used the fact that the height variance of a plane wave is $\frac{1}{2}a^2$ and that the significant wave height is defined as four times the root-mean-square height. The offset is therefore comparable to the mesoscale signal (order 10 cm) and greater than SWOT's precision. It varies in time as the wave properties evolve, so it is indispensable to close the budget (5). The residual $h'_g - h'_a - h'_b - h'_s$ should not vanish but equal the Stokes offset (with its average over the time series removed).

Once the surface gravity waves are averaged out, the barometrically corrected surface height $h'_g - h'_a$ is dominated by the external tides with an amplitude on the order of 1 m (Fig. 3a). As expected, this tidal signal is largely mirrored in the bottom pressure. The residual $h'_g - h'_a - h'_b$ is reduced in amplitude to about 10 cm and exhibits prominent variations on a time scale of a month or two (Fig. 3b). This signal is due to mesoscale eddies moving across the mooring (Wang et al., 2022; de Marez et al., 2023). It is also

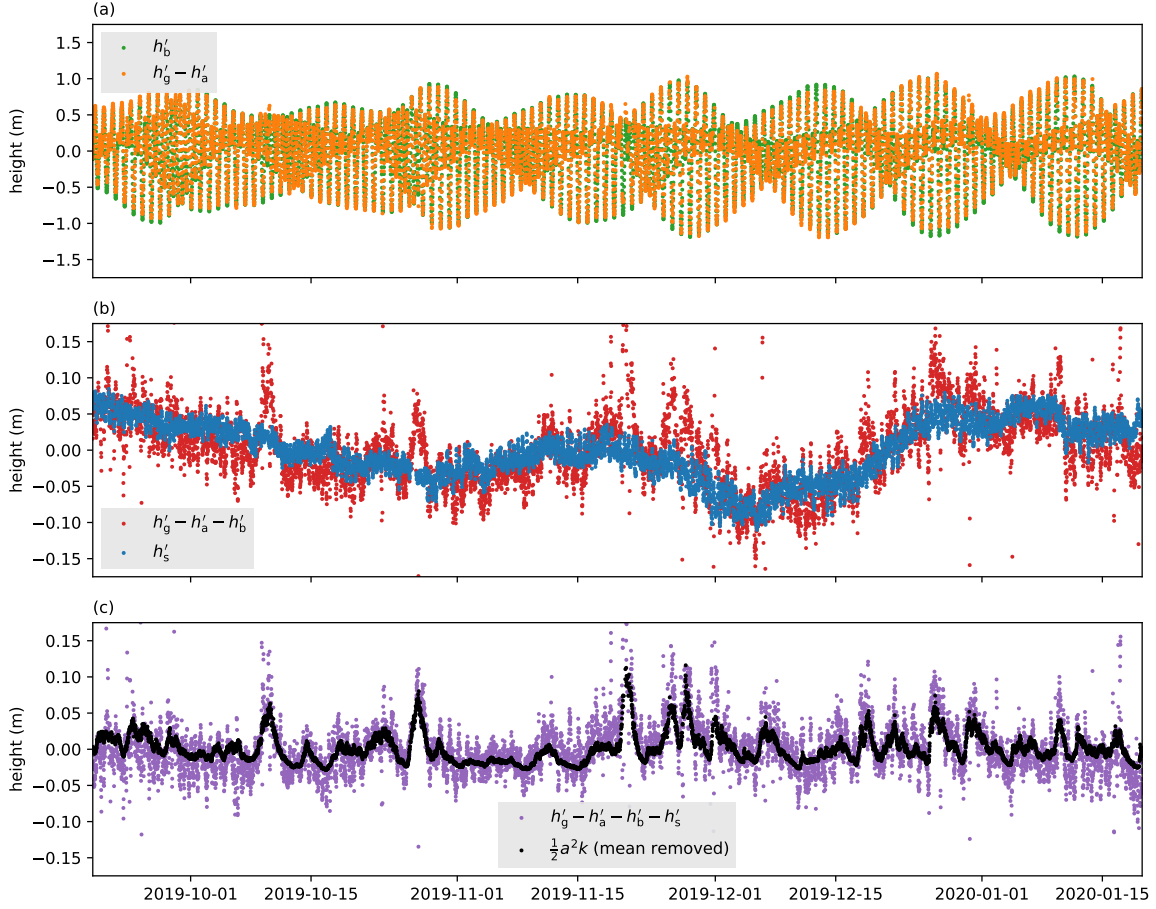


Figure 3: Closure of the sea surface height budget by the Stokes offset. (a) The height equivalent to the bottom pressure h'_b inferred from the bottom pressure recorder and the barometrically corrected surface height $h'_g - h'_a$ inferred from the GPS buoy and corrected using atmospheric reanalysis. (b) Residual $h'_g - h'_a - h'_b$ and the steric height h'_s inferred from CTDs along the mooring line. (c) Residual of the sea surface height budget $h'_g - h'_a - h'_b - h'_s$ and the Stokes offset $\frac{1}{2}a^2k$ calculated from the wave properties estimated from the GPS buoy and with a time mean over the observational period removed.

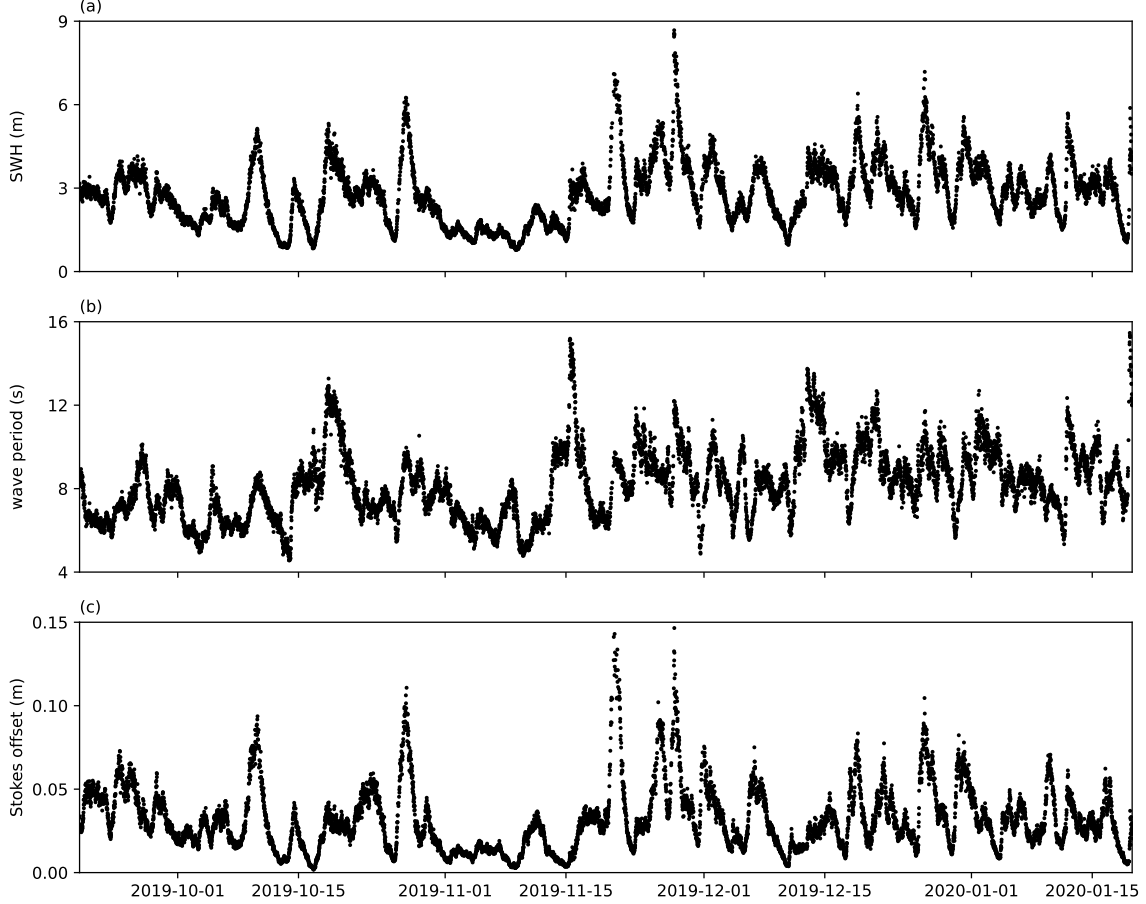


Figure 4: Wave properties and the Stokes offset. (a) Significant wave height η calculated as four times the standard deviation of the GPS buoy measurements. (b) Dominant wave period $2\pi/\omega$ calculated from the power spectral density of the surface height measured by the GPS buoy. (c) Stokes offset estimated as $\frac{1}{2}a^2k = \frac{1}{16}\eta^2k$.

captured by the steric height h'_s , as expected from the sea surface height balance (5). The time series $h'_g - h'_a - h'_b$ has more variance than h'_s at high frequencies and a number of outliers, which we make no attempt to remove. Nevertheless, it is clear that there are systematic differences between the two in the form of spikes in $h'_g - h'_a - h'_b$ that last a few days and are absent in h'_s . These spikes are prominent in the residual of the sea surface height budget $h'_g - h'_a - h'_b - h'_s$ (Fig. 3c). They coincide with periods of large-amplitude surface gravity waves, when the Stokes offset is large.

We estimate the wave properties by calculating the significant wave height η as four times the standard deviation of the barometrically corrected surface height from the GPS

buoy over the 20-minute averaging periods (Fig. 4a). We calculate the dominant wave period by estimating the power spectral density $S(\sigma)$ for each 20-minute period and calculating $\omega = \int \sigma S(\sigma) d\sigma / \int S(\sigma) d\sigma$ (Fig. 2). The dominant wave period $2\pi/\omega$ is on the order of 10 s but shows substantial variations over the observational period (Fig. 4b). We obtain the wavenumber from the dispersion relation of deep-water waves, $k = \omega^2/g$, and calculate the Stokes offset as $\frac{1}{16}\eta^2k$, assuming that the wave field is dominated by a single plane wave. This offset varies primarily because of variations in the wave amplitude and secondarily because of variations in the wave period (Fig. 4c).

This Stokes offset, despite the simplifying assumptions made in calculating it, matches the residual of the sea surface height budget $h'_g - h'_a - h'_b - h'_s$ remarkably well (Fig. 3c). The peaks in the residual line up with periods of large-amplitude waves, when the Stokes offset is large. The height of the peaks matches well, and we emphasize that there is no adjustable parameter in this calculation. This demonstrates the importance of the Stokes offset in the closure of the sea surface height budget if the surface height is measured using a buoy that behaves largely like a Lagrangian particle in the surface gravity wave field.

3 Discussion

The empirical correction of an apparent sea state bias that Wang et al. (2022) applied to the GPS buoy measurements is likely dominated by the Stokes offset. A linearization of the Stokes offset $\frac{1}{16}\eta^2k$ at mean wave conditions yields a proportionality constant of $\frac{1}{8}\eta k = 0.021$, not far from the 0.018 that Wang et al. (2022) inferred from a linear fit to the GPS measurements against η . That said, other sea state-dependent errors in the GPS solution, for example, changes in the effective elevation cutoff (cf., Park and Won, 2010) from the varying wave field, cannot be dismissed and warrant further investigation.

We calculated the Stokes offset using the assumption of a single plane wave. While the real wave field is often dominated by a single swell, for which this assumption is reasonable, this is not universally true. The estimate for the Stokes offset could be refined by calculating it using a superposition of two waves or a whole broadband spectrum of waves. Given the good agreement with the residual using the plane-wave estimate (Fig. 3c), we do not attempt this here. If seeking an accurate correction of the Stokes offset, however, to compare GPS and altimetry measurements, for example, the full wave field should be taken into account.

In our calculation, we also assumed that the GPS buoy perfectly follows the wave

orbit. We expect this to be approximately true given the slack mooring design, but the line tension will cause deviations from the wave orbit, especially when the buoy is displaced farthest from the anchor (Fig. 1). The line tension is recorded on the GPS buoy, so it should be possible to correct for this effect. Again, this does not appear to change the leading-order behavior but should be evaluated in more detail in future work aiming for a quantitatively accurate correction for the Stokes offset.

There are signals in the residual of the sea surface height budget that are not explained by the Stokes offset, including a high-frequency signal contributed by the GPS data (Fig. 3c). Clearly, errors persist in all measurements, and we refer the reader to Wang et al. (2022) for an in-depth discussion. Errors in the GPS measurements due to atmospheric refraction and the incomplete coverage of the water column by CTDs (Fig. 1) are likely major contributors to the remaining residual.

Elipot (2020) recently proposed to supplement the global sea level measurements from altimetry and tide gauges with GPS measurements from drifting buoys, such as those deployed by NOAA's Global Drifter Program. The Stokes offset should be taken into account in such measurements to the extent that the drifting buoys follow the wave orbit. This is particularly important because substantial trends in wave height—and therefore the Stokes offset—are expected for the 21st century (e.g., Casas-Prat et al., 2024).

Acknowledgments

This research was carried out in part at the Jet Propulsion Laboratory, California Institute of Technology, under a contract with the National Aeronautics and Space Administration (80NM0018D0004). The work was supported in part by NASA grants No. 80NSSC20K1140 and 80NSSC24K1652 to the California Institute of Technology.

Data availability statement

All data can be obtained from NASA's Physical Oceanography Distributed Active Archive Center. The GPS buoy data can be accessed at <https://doi.org/10.5067/SWTPR-GPS01>, the mooring CTD data at <https://doi.org/10.5067/SWTPR-CTD11>, and the bottom pressure recorder data at <https://doi.org/10.5067/SWTPR-BPR01>. The ERA5 data is available from the Copernicus Climate Data Store at <https://doi.org/10.24381/cds.adbb2d47>.

References

- Bühler, O. (2014) *Waves and Mean Flows*. 2nd ed. Cambridge University Press. 360 pp.
- Casas-Prat, M. et al. (2024) Wind-Wave Climate Changes and Their Impacts. *Nature Reviews Earth & Environment* 5 (1), 23–42.
- Cazenave, A., W. Llovel (2010) Contemporary Sea Level Rise. *Annual Review of Marine Science* 2, 145–173.
- Chelton, D. B., M. G. Schlax, R. M. Samelson (2011) Global Observations of Nonlinear Mesoscale Eddies. *Progress in Oceanography* 91 (2), 167–216.
- De Marez, C., J. Callies, B. Haines, D. Rodriguez-Chavez, J. Wang (2023) Observational Constraints on the Submesoscale Sea Surface Height Variance of Balanced Motion. *Journal of Physical Oceanography* 53 (5), 1221–1235.
- Desai, S., B. Haines, C. Meinig, S. Stalin (2018) *Status, Results, and Plans for Development of GPS Buoys: Potential for SWOT in-Situ CALVAL*. Version 2. Root.
- Egbert, G. D., R. D. Ray (2000) Significant Dissipation of Tidal Energy in the Deep Ocean Inferred from Satellite Altimeter Data. *Nature* 405 (6788), 775–778.
- Elipot, S. (2020) Measuring Global Mean Sea Level Changes with Surface Drifting Buoys. *Geophysical Research Letters* 47 (21), e2020GL091078.
- Fu, L.-L. et al. (2024) The Surface Water and Ocean Topography Mission: A Breakthrough in Radar Remote Sensing of the Ocean and Land Surface Water. *Geophysical Research Letters* 51 (4), e2023GL107652.
- Gill, A. E., P. P. Niiler (1973) The Theory of the Seasonal Variability in the Ocean. *Deep Sea Research and Oceanographic Abstracts* 20 (2), 141–177.
- Haines, B., S. Desai, A. Dodge, B. Leben, M. Shannon, C. Meinig, S. Stalin (2019) *The Harvest Experiment: New Results from the Platform and Moored GPS Buoys*. Version 3. Root.
- Haines, B., S. Desai, C. Meinig, S. Stalin (2017) *CALVAL of the SWOT SSH Spectrum: Moored GPS Buoy Approach*. Version 2. Root.
- Le Provost, C., A. F. Bennett, D. E. Cartwright (1995) Ocean Tides for and from TOPEX/POSEIDON. *Science* 267 (5198), 639–642.
- Longuet-Higgins, M. S. (1986) Eulerian and Lagrangian Aspects of Surface Waves. *Journal of Fluid Mechanics* 173, 683–707.
- Munk, W., C. Wunsch (1998) Abyssal Recipes II: Energetics of Tidal and Wind Mixing. *Deep Sea Research Part I: Oceanographic Research Papers* 45 (12), 1977–2010.

- Park, K.-D., J. Won (2010) The Foliage Effect on the Height Time Series from Permanent GPS Stations. *Earth, Planets and Space* 62 (11), 849–856.
- Ray, R. D., G. T. Mitchum (1996) Surface Manifestation of Internal Tides Generated near Hawaii. *Geophysical Research Letters* 23 (16), 2101–2104.
- Salmon, R. (2020) *More Lectures on Geophysical Fluid Dynamics*.
- Wang, J. et al. (2022) On the Development of SWOT in Situ Calibration/Validation for Short-Wavelength Ocean Topography. *Journal of Atmospheric and Oceanic Technology* 39 (5), 595–617.
- Wunsch, C., D. Stammer (1997) Atmospheric Loading and the Oceanic “Inverted Barometer” Effect. *Reviews of Geophysics* 35 (1), 79–107.
- Wunsch, C., D. Stammer (1998) Satellite Altimetry, the Marine Geoid, and the Oceanic General Circulation. *Annual Review of Earth and Planetary Sciences* 26 (1), 219–253.